Int. J. Heat Mass Transfer. Vol. 36, No. 15, pp. 3759–3764, 1993
Printed in Great Britain

0017-9310/93 $6.00 + 0.00

An efficient computational technique to solve the moving boundary problems in the axisymmetric geometries

CHARN-JUNG KIM, SUNG TACK RO† and JOON SIK LEE
Department of Mechanical Engineering, Seoul National University, Seoul 151-742, Korea

(*Received* 18 *May* 1992 *and in final form* 5 *March* 1993)

Abstract—A computational technique was set forth with the aid of the boundary immobilization technique to treat the moving boundary problems occurring in the axisymmetric geometries. The use of a geometry index allowed the present method to share many of the features with an existing numerical method developed for the planar geometry. A key feature of the present work was that the numerical formulation of the pseudo-velocities arising from the boundary immobilization was not derived, as in the conventional approaches, directly from the mathematical expressions but based on the physical meanings pertaining to them. Therefore, the numerical values of the pseudo-velocities and the time-dependent volume elements were determined algebraically instead of solving the field equation for the pseudo-velocities. Several notable advantages such as the facility in the numerical implementation and the independence of the coordinate systems would be corroborative of the application potentials of the present method to a variety of moving boundary problems.

1. INTRODUCTION

AMONG a large collection of numerical analyses on moving boundary problems, the boundary immobilization technique has been widely used owing to its crucial advantage of working with fixed computational domains. A survey of the literature indicates that in contrast to the abundance of publications concerning planar geometry moving boundary problems in *axisymmetric* geometries have attracted less attention of researchers (e.g. in refs. [1–3]).

Recently developed in ref. [4] is a numerical method which is strongly consistent with the well-established finite-volume integration method [5] used for fixed boundary problems. However, the development in ref. [4] is confined to planar geometry. The motivation of the present study is to further extend their method to take axisymmetric geometry into consideration. Therefore, the major aim of this study will be directed to highlight the special features due to the axisymmetric geometry.

A dilemma encountered in using the boundary immobilization techniques is that the pseudo-velocities (or the mesh velocities) arising from the boundary immobilization need to be discretized in such a way that the global mass conservation can be preserved. Being aware of this nuisance, Thomas and Lombard [6] formulate the geometric conservation law that governs the time variation of the spatial volume element, and they solve it numerically along with the flow conservation equations. They presume that the failure to satisfy the geometric conservation law triggers the grid motion-induced errors and thus is responsible for the oscillations and instabilities encountered in ref. [7]. Although their approach is more rigorous than other methods from the standpoint of the conservation principles, it is still cumbersome to solve the additional field equation. In the present study, the numerical values of the pseudo-velocities and of the time-dependent volume elements are algebraically determined from a self-satisfactory geometrical relation instead of solving the differential geometric conservation equation. Consequently, the method presented here can serve as an efficient tool in treating a broad class of complicated problems with moving boundaries.

† Author to whom correspondence should be addressed.

2. NUMERICAL FORMULATION

In this section, a computational method applicable to both the planar and axisymmetric moving-boundary problems is described. In order to work with the two different coordinate systems in a unified approach, we use only one pair of x and y to denote spatial independent variables for both the systems. In the case of an axisymmetric geometry, the x-coordinate is aligned with the radial direction and the y-coordinate with the axial direction.

2.1. *Governing equations*

We write the conservation equation for a general dependent variable ϕ as

$$\frac{\partial}{\partial t}(x^n\rho\phi)+\frac{\partial}{\partial x}\left(x^n\rho u\phi-x^n\Gamma\frac{\partial\phi}{\partial x}\right)+\frac{\partial}{\partial y}\left(x^n\rho v\phi-x^n\Gamma\frac{\partial\phi}{\partial y}\right)=x^nS(x,y) \quad (1)$$

NOMENCLATURE

$\hat{F}$	mass flux at interface
h_{sf}	latent heat [J kg^{-1}]
H	tube height [m]
J	Jacobian or flux of ϕ
Pr	Prandtl number, ν/α
$\dot{Q}_w$	heat transfer rate at the tube wall
Ra	Rayleigh number, $g\beta_T\Delta T x_w^3/\alpha\nu$
Ste	Stefan number, $c(T_w-T_m)/h_{sf}$
t	time [s]
T_m	melting temperature [K]
T_w	tube wall temperature [K]
u_ξ, u_η	covariant velocity components [m s^{-1}]
x, y	spatial independent variables [m]
x_w	outer radius of the tube [m]
x_m	interface position [m]
$\tilde{X}_t$, $\tilde{Y}_t$	axisymmetric terms.

Greek symbols

α	thermal diffusivity [m^2 s^{-1}]
δ	thickness of melt region, x_m-x_w [m]
ξ, η	dimensionless transformed coordinates
τ	dimensionless time, $(\nu t/x_w^2)Ste/Pr$.

Superscripts

$+$	dimensionless
$\sim$	axisymmetric
$\hat{}$	interface.

Subscripts

L	liquid
S	solid.

where the geometry index n has a value of 0 for the planar and 1 for the axisymmetric coordinate systems; the density ρ is assumed to be constant within each physical domain of interest.

In order to overcome computational difficulties in accounting for moving boundaries of irregular shape, a general curvilinear coordinate system

$$x = x(\xi,\eta,t), \quad y = y(\xi,\eta,t) \tag{2}$$

is introduced such that the moving boundaries are immobilized in the new (ξ,η) coordinate at all times. Equation (1) is then transformed into

$$\frac{\partial}{\partial t}(\tilde{J}\rho\phi)+\frac{\partial}{\partial\xi}\left(\rho U\phi-\frac{\alpha_\xi\Gamma}{h_\xi}\frac{\partial\phi}{\partial\xi}\right)+\frac{\partial}{\partial\eta}\left(\rho V\phi-\frac{\alpha_\eta\Gamma}{h_\eta}\frac{\partial\phi}{\partial\eta}\right)$$
$$=\tilde{J}S(\xi,\eta)-\frac{\partial}{\partial\xi}\left(\frac{\beta_\xi\Gamma}{h_\eta}\frac{\partial\phi}{\partial\eta}\right)-\frac{\partial}{\partial\eta}\left(\frac{\beta_\eta\Gamma}{h_\xi}\frac{\partial\phi}{\partial\xi}\right) \tag{3}$$

where

$$U=\alpha_\xi u_\xi-\beta_\xi u_\eta-\tilde{X}_t, \quad V=\alpha_\eta u_\eta-\beta_\eta u_\xi-\tilde{Y}_t \tag{4}$$
$$\tilde{J}=x^nJ, \quad \tilde{X}_t=x^nX_t, \quad \tilde{Y}_t=x^nY_t \tag{5}$$
$$\alpha_\xi=x^nh_\xi h_\eta^2/J, \quad \alpha_\eta=x^nh_\eta h_\xi^2/J \tag{6}$$
$$\beta_\xi=x^n\lambda h_\eta/J, \quad \beta_\eta=x^n\lambda h_\xi/J \tag{7}$$
$$h_\xi=(x_\xi^2+y_\xi^2)^{1/2}, \quad h_\eta=(x_\eta^2+y_\eta^2)^{1/2} \tag{8}$$
$$\lambda=x_\xi x_\eta+y_\xi y_\eta, \quad J=x_\xi y_\eta-y_\xi x_\eta \tag{9}$$
$$X_t=y_\eta x_t-x_\eta y_t, \quad Y_t=x_\xi y_t-y_\xi x_t \tag{10}$$
$$u_\xi=(x_\xi u+y_\xi v)/h_\xi, \quad u_\eta=(x_\eta u+y_\eta v)/h_\eta. \tag{11}$$

Here, it needs to be emphasized that the axisymmetric factor x^n is individually included in the tilded terms and in the α_ξ, α_η, β_ξ and β_η terms. The rationale for this unique treatment is based on the dual evaluation of x^n, which will be discussed later. Since the computational strategy to solve a set of equations (3)–(11) for the case of planar geometry was already discussed in ref. [4], focus will be now placed on the treatment of equations (5)–(7) into which the effect of the axisymmetric geometry is incorporated.

2.2. *Evaluation of the volume elements*

In the axisymmetric case, the physical control volume becomes a body of revolution. Referring to Fig. 1 and dropping the constant factor of 2π, the volume of the body of revolution generated by rotating triangle ABD along the y-axis, $\tilde{m}$(ABD), can be expressed as

$$\tilde{m}(\mathrm{ABD})=\bar{x}_{\mathrm{ABD}}m(\mathrm{ABD}) \tag{12}$$

where $\bar{x}_{\mathrm{ABD}}$ is the x-coordinate of the moment center of triangle ABD

$$\bar{x}_{\mathrm{ABD}}=\frac{1}{3}(x_A+x_B+x_D) \tag{13}$$

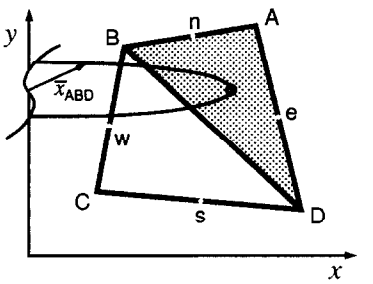

FIG. 1. A finite control volume in the physical (x, y) coordinate. An axisymmetric case is shown in the figure where the axis of revolution is the y-coordinate.

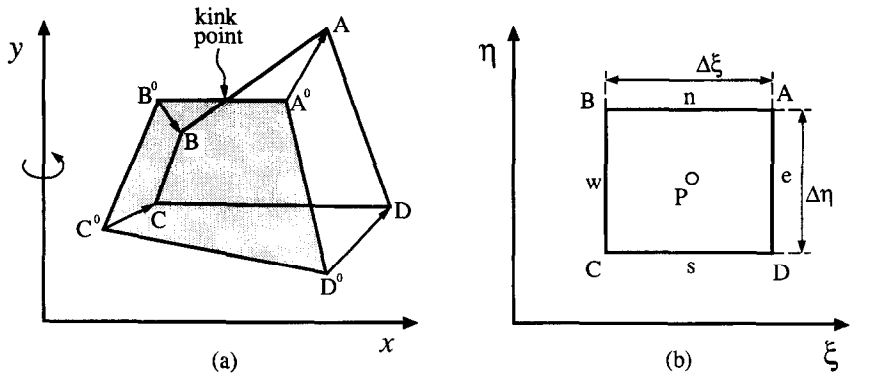

FIG. 2. Schematic diagram of finite control volumes at two consecutive time steps: (a) in the physical space, (b) in the computational space. The points e, w, n and s designate face centers.

and $m(\mathrm{ABD})$ is the area of triangle ABD

$$m(\mathrm{ABD}) = \frac{1}{2}\begin{Bmatrix} x_A & x_B & x_D & x_A \\ y_A & y_B & y_D & y_A \end{Bmatrix} \equiv \frac{1}{2}(x_A y_B + x_B y_D + x_D y_A - x_B y_A - x_D y_B - x_A y_D). \quad (14)$$

Note that $m(\mathrm{ABD})$ assumes a positive value when ABD is traced counterclockwise and a negative value otherwise, i.e. $m(\mathrm{ABD}) = -m(\mathrm{ADB})$. Then, the volume $\tilde{m}(\mathrm{ABCD})$ becomes

$$\tilde{m}(\mathrm{ABCD}) = \tilde{m}(\mathrm{ABD}) + \tilde{m}(\mathrm{BCD}) \quad (15)$$

where $\tilde{m}(\mathrm{BCD})$ can be determined similarly.

Figure 2(a) illustrates two quadrangles that represent the physical control volumes at two consecutive time steps with $\mathrm{A^0B^0C^0D^0}$ at time t^0 and ABCD at time $t^0 + \Delta t$. The volume $\tilde{m}(\mathrm{B^0A^0AB})$ that is generated by rectangle $\mathrm{B^0A^0AB}$ is obtained similar to equation (15):

$$\tilde{m}(\mathrm{B^0A^0AB}) = \tilde{m}(\mathrm{B^0A^0A}) + \tilde{m}(\mathrm{B^0AB}). \quad (16)$$

In case quadrangle $\mathrm{B^0A^0AB}$ has a kink point as shown in Fig. 2(a), we have $\tilde{m}(\mathrm{B^0A^0A}) > 0$ and $\tilde{m}(\mathrm{B^0AB}) < 0$. The presence of such a kink point during the movement of a physical control volume can be interpreted that both the pseudo-inflow and the pseudo-outflow are imposed on the face of a stationary computational control volume (cf. the north face in Fig. 2(a)). This delicate situation clearly explains the reason why each control volume has been split into two volumes of triangular sections to determine its magnitude.

For the two control volumes shown in Fig. 2(a), it is easily found that

$$\tilde{m}(\mathrm{ABCD}) - \tilde{m}(\mathrm{A^0B^0C^0D^0}) = \tilde{m}(\mathrm{A^0D^0DA}) - \tilde{m}(\mathrm{B^0C^0CB}) + \tilde{m}(\mathrm{B^0A^0AB}) - \tilde{m}(\mathrm{C^0D^0DC}) \quad (17)$$

which has a familiarity with the area rule [4] and, therefore, will be provisionally called here the *extended area rule*. Not surprisingly, equation (17) is self-satisfactory since it is just derived from a purely geometrical point of view.

2.3. *Discretization of the pseudo-velocities*

One peculiar aspect of the boundary immobilization techniques is that they inherently create the pseudo-velocities in the transformed equations. The existence of these pseudo-velocities induces an additional condition, often known as the geometric conservation law, that needs to be satisfied. The geometric conservation law has been obtained from the Reynolds transport theorem to give [6]

$$\frac{\partial \tilde{J}}{\partial t} = \frac{\partial \tilde{X}_t}{\partial \xi} + \frac{\partial \tilde{Y}_t}{\partial \eta} \quad (18)$$

which can be alternatively deduced from equation (3) using $\rho = \phi = 1$ and $u = v = S = 0$ [6]. By integrating equation (18) over a finite computational control volume shown in Fig. 2(b) and over a finite time increment, we have

$$\tilde{J}_P \Delta\xi \cdot \Delta\eta - \tilde{J}_P^0 \Delta\xi \cdot \Delta\eta = \tilde{X}_{t,e} \Delta\eta \cdot \Delta t - \tilde{X}_{t,w} \Delta\eta \cdot \Delta t + \tilde{Y}_{t,n} \Delta\xi \cdot \Delta t - \tilde{Y}_{t,s} \Delta\xi \cdot \Delta t \quad (19)$$

which is by no means as self-satisfactory as the above-mentioned extended area rule.

While the extended area rule reflects the same physical concept as the discretized version of the geometric conservation law, the former precedes the latter. In this regard, we now seek the discretization expressions of $\tilde{J}$, $\tilde{X}_t$ and $\tilde{Y}_t$ from the self-satisfactory, extended area rule in order to preserve the global mass conservation. Therefore, we equate each term in equation (17) with the corresponding term in equation (19) such that

$$\begin{aligned} \tilde{J}_P \Delta\xi \cdot \Delta\eta &= \tilde{m}(\mathrm{ABCD}) \\ \tilde{X}_{t,e} \Delta\eta \cdot \Delta t &= \tilde{m}(\mathrm{A^0D^0DA}) \\ \tilde{Y}_{t,n} \Delta\xi \cdot \Delta t &= \tilde{m}(\mathrm{B^0A^0AB}) \end{aligned} \quad (20)$$

with other terms expressed in a similar way. As for equation (20), it should be recognized that the axisymmetric factor x^n in the $\tilde{X}_t$ and $\tilde{Y}_t$ terms has been evaluated neither at the old time nor at the current time. In fact, an essence of the present formulation is that the

discretization of the $\tilde{X}_\xi$ and $\tilde{Y}_\eta$ terms is based on the physical instead of mathematical concepts.

However, in accordance with the implicit discretization scheme, the geometric terms unrelated to the movement of the physical control volume—i.e. α_ξ, α_η, β_ξ and β_η—should be evaluated at the current time level. This *dual* evaluation of the geometric factors can be justified from the fact that both the physical velocity and the pseudo-velocity fields satisfy independently the transformed mass continuity equation.

A strong attraction of the present work lies in the fact that, when the extra terms due to the axisymmetric geometry are handled as explained above, both the planar and axisymmetric moving-boundary problems can be taken into consideration in a unified way. Therefore, no further discussion on the discretization procedure will be made from this point on; the potential users of this method are referred to ref. [4] for further information.

3. EXAMPLE PROBLEM

An example problem is taken from the numerical analysis of Sparrow *et al.* [1] which stands for the first numerical simulation accounting for the natural convection within the melt. Since the primary emphasis here is on the presentation of a computational technique, only a brief treatment is given below and a detailed investigation of the problem considered can be found elsewhere [8].

3.1. *Problem description*

A tube of height H and outer radius x_w is embedded vertically in a solid, as shown in Fig. 3, and the top and bottom surfaces bounding the system are insulated. The entire system is initially at the melting temperature T_m. At time $t = 0$, the temperature of the outer surface of the tube is raised to a fixed value of $T_w > T_m$. Then, the melting front x_m starts to move away from the tube wall and, after sufficient elapsed times, results in a curved surface due to the dominance of natural convection over conduction. The difference between the solid and liquid densities is neglected.

Numerical simulation is initiated using the following coordinate transformation:

$$x = x_w + \delta\xi, \quad y = H\eta \tag{21}$$

where $\delta = x_m - x_w$ and the region $0 \leqslant \xi, \eta \leqslant 1$ consists of the computational domain. Table 1 summarizes the dimensionless governing equations into which the assumption of laminar natural convection is incorporated. The boundary conditions except the interface are

$$T = T_w \quad \text{at} \quad \xi = 0; \quad T = T_m \quad \text{at} \quad \xi = 1$$
$$\partial T/\partial y^+ = 0 \quad \text{at} \quad \eta = 0, 1$$
$$u = v = 0 \quad \text{at} \quad \xi = 0, 1 \text{ and } \eta = 0, 1. \tag{22}$$

The dimensionless parameters characterizing this problem are Pr, Ra, Ste and H/x_w.

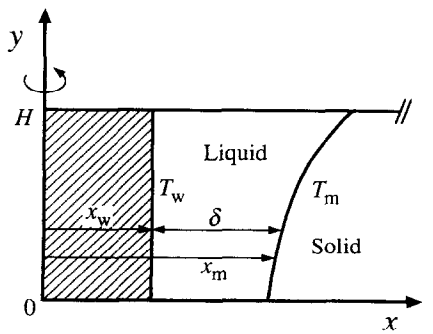

FIG. 3. An illustration of the example phase-change problem in the axisymmetric geometry.

Table 1. Variables in the dimensionless governing equations. Here, $\rho^+ = 1$, $t^+ = \nu t/x_w^2$, $x^+ = x/x_w$, $r^+ = r/x_w$, $u^+ = ux_w/\nu$, $v^+ = vx_w/\nu$, $p^+ = px_w^2/\rho\nu^2$, and $\theta = (T - T_m)/(T_w - T_m)$

	ϕ^+	Γ^+	S^+
Continuity	1	0	0
Momentum	u^+	1	$-\partial p^+/\partial x^+ - u^+/x^{+2}$
	v^+	1	$-\partial p^+/\partial y^+ + (Ra/Pr)\theta$
Energy	θ	$1/Pr$	0

3.2. *Treatment of the moving interface*

The interfacial conditions can be directly derived from the transformed conservation equation considering the continuity condition of fluxes crossing the interface [4]. In this matter, we introduce F and J

$$F = \rho U, \quad J = Fh - \frac{\alpha_\xi k}{h_\xi}\frac{\partial T}{\partial \xi} + \frac{\beta_\xi k}{h_\eta}\frac{\partial T}{\partial \eta} \tag{23}$$

so that the interfacial mass and energy balances are expressed as [4]

$$\hat{F}_L = \hat{F}_S \equiv \hat{F}, \quad \hat{J}_L = \hat{J}_S. \tag{24}$$

The interfacial energy balance, $\hat{J}_L = \hat{J}_S$, is then discretized to obtain the value of $\hat{F}$ from which the interface movement can be determined explicitly (for details, see ref. [4]). After all the $\hat{F}$ values are calculated along the interface, $u_\xi = u_\eta = 0$ conditions at the interface and $y_t = 0$ are used to get

$$\hat{F} = -\rho x(y_\eta x_t) \quad \text{or} \quad \frac{\partial x^2}{\partial t} = -\frac{2\hat{F}}{\rho y_\eta} \tag{25}$$

which can be discretized immediately to obtain the new interface position. Especially, the interface conditions at $\eta = 0$ and $\eta = 1$ can be separately derived from the adiabatic conditions, i.e.

$$\rho Vh - \frac{\alpha_\eta k}{h_\eta}\frac{\partial T}{\partial \eta} + \frac{\beta_\eta k}{h_\xi}\frac{\partial T}{\partial \xi} = 0$$
$$\text{at } \eta = 0, 1 \text{ and } \xi = 1 \tag{26}$$

the first terms of which are identically zero (due to the

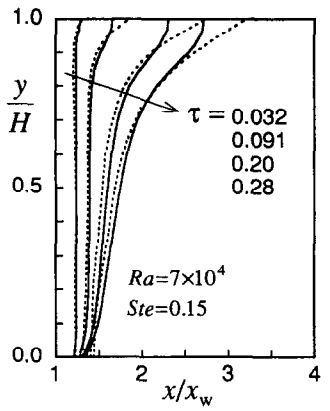

FIG. 4. Numerical results for the interface positions for the case of $H/x_w = 4$, $Ste = 0.15$ and $Ra = 7 \times 10^4$. This work (solid lines); Sparrow *et al.* [1] (dotted lines).

impermeable surface and the isotherm of interface). Then, we have $\beta_\eta = 0$ since $\partial T/\partial \xi$, $h_\xi \neq 0$. The condition $\beta_\eta = 0$ means that the interface should intersect orthogonally with the bounding surfaces (or $d\delta/dy = 0$ at $\eta = 0$ and $\eta = 1$). However, in the present computation, the interface positions at these points are rather linearly extrapolated for a comparative study.

3.3. *Numerical results*

A nonuniform 23×31 grid system is used for computation. To remove the start-up difficulty, the liquid phase of thickness $\delta/x_w = 0.01$ is assumed to exist initially. At any instant of time, computed solutions are assumed to have converged when the maximum value of normalized residues becomes less than 10^{-5}. The overall energy balance proves to be valid within a tolerance of 1% throughout the results presented below.

Numerical results are mainly obtained with $Pr = 7$; $H/x_w = 4$, 10; and for three different Rayleigh numbers, $Ra = 7 \times 10^4$, 7×10^5, 7×10^6. In Fig. 4, the predicted interface positions at several elapsed times for $H/x_w = 4$, $Ste = 0.15$ and $Ra = 7 \times 10^4$ are displayed. As opposed to the monotonically increasing slope of the interfaces from ref. [1], our results show the presence of an inflection point and depict nearly zero slopes at both the bottom and the top of the melt region. This leveling-off behavior appears to be mainly caused by the inclusion of the nonorthogonal terms, because the zero-slope condition at the bounding surfaces was not implemented in the present computation, as was mentioned earlier. We point out that the experiments in the planar geometry [9] have confirmed this gradually vanishing slope of the interface near the top adiabatic surface. For the parameters specified above, we believe that agreement between the two results is in general satisfactory in view of the frontier character of the work done in ref. [1].

The interface positions for the higher Rayleigh numbers are portrayed in Fig. 5. When compared with the above case corresponding to a smaller Ra, the time evolution of the interface proceeds substantially faster near the top adiabatic surface, while below the middle it is rather insensitive to Ra. The results shown in Figs. 4 and 5 are indicative of the melting trend in response to the variation of Ra, i.e. the melt region is concentrated more toward the top for higher values of Ra as indicated by the fact that the interface shape and its evolution are strongly influenced by the Rayleigh number in the upper portion but not so intensely in the lower portion. However, this observation is contradictory to that of ref. [1] in which it is claimed that the interface slope tends to be more or less uniform with an increasing Ra (see Fig. 5 in ref. [1]). It is uncertain that such a discrepancy at a high Ra is primarily due to the relatively coarse (12×14) grid system used there. Meanwhile, Fig. 5(a) shows that the numerical results from this study are fairly consistent with those from ref. [8]. A small disagreement with the results of ref. [8] is expected due to the inclusion of the pseudo-velocities in the present study.

Figure 6 illustrates the general characteristics of the flow and the isotherm patterns at two selected times.

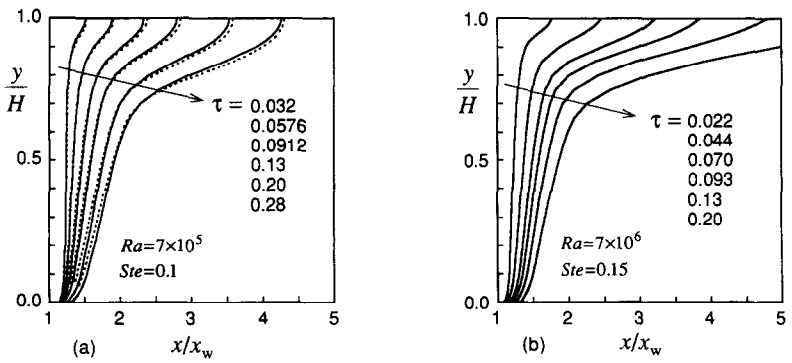

FIG. 5. The predicted interface shape and its evolution for the case of $H/x_w = 4$. (a) $Ste = 0.1$ and $Ra = 7 \times 10^5$ (or $Ra_H = 4.5 \times 10^7$ based on the height); (b) $Ste = 0.15$ and $Ra = 7 \times 10^6$. This work (solid lines); Hossfeld [8] (dotted lines).

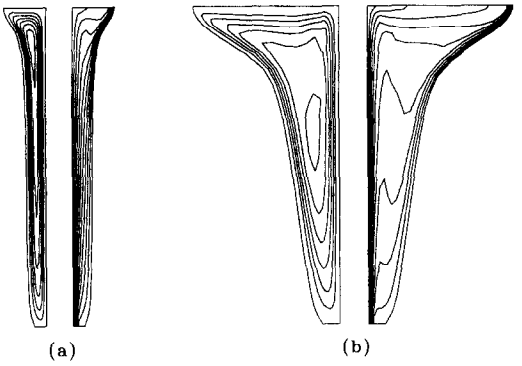

FIG. 6. Streamline (left) and isotherm (right) patterns for $H/x_w = 4$, $Ra = 7 \times 10^5$ and $Ste = 0.1$, (a) at $\tau = 0.032$ and (b) at $\tau = 0.13$. The iso-lines are drawn with equal increments.

Streamlines are drawn with the aid of the stream-function defined as

$$\frac{\partial \psi}{\partial \eta} = U + \tilde{X}_f, \quad -\frac{\partial \psi}{\partial \xi} = V + \tilde{Y}_f. \tag{27}$$

The isotherm distribution reveals that large gradients of temperature are localized both near the top interface and close to the bottom tube, which is responsible for the melting pattern shown in Figs. 4 and 5.

Figure 7 exhibits the transient heat transfer rate per unit length of the tube for three different Rayleigh numbers and two height–radius ratios. The pure conduction solution (i.e. with $Ra = 0$) is also shown to illustrate the relative importance of the natural convection. At small times all the curves collapse well onto the conduction-curve, thereby reaffirming an established fact that conduction plays a predominant role of heat transfer mechanism at early melting. Also noted are that as Ra increases the detachment from the conduction-curve takes place earlier, and that the average heat transfer rate per unit length is higher for a tube with a smaller H/x_w value. This heat transfer characteristic may be very useful in the overall design of this type of thermal energy storage system [8]. A striking difference from Fig. 2 of ref. [1] is that the present work does not show any indication of the temporal maximum value in the average heat transfer rate. This discrepancy seems due to the different resolution of the grid system employed (cf. Fig. 23 in ref. [8]).

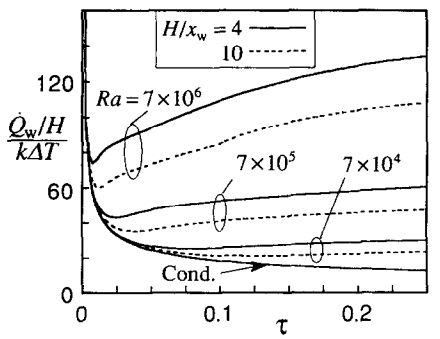

FIG. 7. The dimensionless heat transfer per unit length of the tube vs the dimensionless time for the case of $Ste = 0.15$. The heat transfer rate at the tube wall, $\dot{Q}_w$, is evaluated from $\dot{Q}_w = \int_0^H -2\pi x_w k(\partial T/\partial x)\,dy$ and $\Delta T = T_w - T_m$.

Acknowledgement—This research was sponsored by the Korea Science and Engineering Foundation (KOSEF).

REFERENCES

1. E. M. Sparrow, S. V. Patankar and S. Ramadhyani, Analysis of melting in the presence of natural convection in the melt region, *J. Heat Transfer* **99**, 520–526 (1977).
2. C. F. Hsu, E. M. Sparrow and S. V. Patankar, Numerical solution of moving boundary problems by boundary immobilization and a control-volume-based finite-difference scheme, *Int. J. Heat Mass Transfer* **24**, 1335–1343 (1981).
3. E. M. Sparrow and Y. Ohkubo, Numerical analysis of two-dimensional transient freezing including solid-phase and tube-wall conduction and liquid-phase natural convection, *Numer. Heat Transfer* **9**, 59–77 (1986).
4. C.-J. Kim and M. Kaviany, A numerical method for phase-change problems with convection and diffusion, *Int. J. Heat Mass Transfer* **35**, 457–467 (1992).
5. S. V. Patankar, *Numerical Heat Transfer and Fluid Flow*. Hemisphere, Washington, D.C. (1980).
6. P. D. Thomas and C. K. Lombard, Geometric conservation law and its application to flow computations on moving grids, *AIAA J.* **17**, 1030–1037 (1979).
7. H. Viviand and W. Ghazzi, Numerical solution of the compressible Navier–Stokes equations at high-*Re* numbers with applications to the blunt body problem, *Lecture notes in Physics* **59**, Springer-Verlag, Berlin (1976).
8. L. M. Hossfeld, A coordinate transformation method for solving a convection phase change problem, Ph.D. Thesis, University of Minnesota, Minneapolis (1979).
9. C. Benard, D. Gobin and A. Zanoli, Moving boundary problem: heat conduction in the solid phase of a phase-change material during melting driven by natural convection in the liquid, *Int. J. Heat Mass Transfer* **29**, 1669–1681 (1986).